Electronic Supplementary Information File

for

Development of high rate-capable O3-structured 'layered' Na transition metal oxide by tuning the cation-oxygen bond covalency

Ishita Biswas[a #], Bachu Sravan Kumar[a #], Anagha Pradeep[a], Arpita Das[a], Velaga Srihari [b], Himanshu K. Poswal [b] and Amartya Mukhopadhyay[a *]

[a]Advanced Batteries and Ceramics Laboratory, Department of Metallurgical Engineering and Materials Science, Indian Institute of Technology Bombay, Mumbai 400076, India

[b] High Pressure and Synchrotron Radiation Physics Division, Bhabha Atomic Research Center, Mumbai 400085, India

* Corresponding author's email ID: amartya_mukhopadhyay@iitb.ac.in

# Equal contributions

Section S1

Material synthesis

The un-doped and Si-doped O3-structured NaT_MO_2s were synthesized by mixing estimated amounts of sodium acetate trihydrate (Sigma Aldrich), lithium acetate dihydrate (Sigma Aldrich), nickel(II) acetate tetrahydrate (Sigma Aldrich), cupric acetate monohydrate (Sigma Aldrich), magnesium nitrate hexahydrate (Sigma Aldrich) and tetra-ethyl orthosilicate (in the case of Si-doped NaT_MO_2) thoroughly, in order to obtain the desired stoichiometry, and dissolving them in de-ionized water by continuously stirring the solution on a hot plate at 85 ^oC till a clear solution was obtained. The titanium but-oxide was initially dissolved in butanol and then added to the precursor solution while stirring. This was followed by adding an optimized quantity of citric acid to the aqueous sol and continuously stirring on a hot plate at 125 ^oC overnight to form a gel. The gel was then heated at 250 ^oC for 1.5 h in a hot air oven to obtain an amorphous solid. The amorphous solid was then ground thoroughly and calcined at 450 ^oC for 2 h to get rid of carbonaceous material. The residue was thoroughly ground and then used for making green pellets by applying a uniaxial pressure of 15 tons. The as-obtained green pellets were then subjected to calcination/annealing at 850 ^oC for 12 h in a tube furnace in air and cooled in Ar atmosphere.

Materials characterizations

Powder X-Ray diffraction (XRD) measurements of the as-synthesized NaT_MO_2s were carried out using PANalytical X'Pert X-ray diffractometer, using Cu Kα radiation, at scan rate of 1 °/min. The XRD patterns were refined using Full Prof Suite software. In order to investigate the chemical compositions (*i.e.,* stoichiometry), inductive coupling plasma – atomic emission spectroscopy (ICP-AES) was carried out using SPECTRO Analytical Instruments (GmbH), with suspensions of 1 mg/mL of the as-synthesized NaT_MO_2s powders in aqua regia. Morphology of the as-synthesized NaT_MO_2s were observed using field emission scanning electron microscope (FEG-SEM; JEOL-JSM7600F). Bright field and high-resolution transmission electron microscopy (HRTEM) of the as-synthesized NaT_MO_2s powders were carried out using JEOL-JEM2100F and Themis 300 G3 (Thermo Scientific), equipped with Fischione 3000 HAADF detector and 'Super-X EDS' detector.

Electrochemical investigations

Electrodes based on the as-synthesized NaT_MO_2s were prepared by homogenously mixing the cathode 'active' materials with carbon black as conducting additive and polyvinylidene fluoride (PVDF) as binder in a ratio of 8:1:1 by mass, respectively. The mixture was ground uniformly for 2 h, mixed with N-Methyl-2-pyrrolidone (NMP) and ground for another 1 h to make a slurry. The cathode slurry was then coated onto Al foil using an automated coating machine, followed by drying in vacuum oven for 12 h, calendaring and punching out electrodes, as per the required dimension (*viz.,* ~14 mm diameter). The mass loading of the electrodes used in the study was ~2-2.5 mg/cm^2.

The electrochemical behavior/performance of the as-synthesized O3-structured NaT_MO_2-based cathode materials were investigated by assembling CR2032 type coin cells in Ar-filled glove box (H_2O and O_2 < 0.1 ppm) with the NaT_MO_2-based cathodes (as working electrode) and metallic Na foil as the counter(anode)-cum-reference electrode in Na 'half' cell arrangement. Whatman glass fibre filter (GF/D) was used as the separator and $NaClO_4$ in EC/PC as the electrolyte. In order to investigate the true and intrinsic performance of the as-designed cathode materials, no special modification or coating was done to the electrode, current collector and electrolyte for 'forcing' good electrochemical performance. Furthermore, the reported first cycle here is the 'true' first cycle without any 'formation cycle' been conducted. Galvanostatic cycling was performed at different current densities within a potential window of 2.0-4.0 V (vs. Na/Na^+) using NEWARE battery tester. Electrochemical impedance spectroscopy (EIS)

and galvanostatic intermittent titration (GITT) were performed using battery tester (Biologic; BCS 810) within 10 mHz - 10 kHz.

Operando synchrotron X-ray diffraction during electrochemical cycling

In order to investigate the possible occurrence(s) of structural/phase transformation(s) of the as-developed Si-doped NaT_MO_2 based cathode material during electrochemical desodiation/sodiation, *operando* studies during galvanostatic cycling were carried out using Extreme conditions - Angle dispersive / Energy dispersive (EC-AD/ED) synchrotron X-ray diffraction (BL11) at Indus-2 beamline (in RRCAT, Indore), with a beam wavelength of 0.69 Å and beam energy of 2.5 GeV. The synchrotron X-ray diffraction patterns, at the open circuit voltage (OCV) and for every 300 s interval during the first galvanostatic charge/discharge cycle @ C/5, were collected on MAR 345 imaging plate, calibrated using CeO_2 standard reference material. The CR2032 coin cells used for these *operando* studies were customized by drilling 3 mm holes on the top case, bottom case and spacer to allow for the beam to pass through. The drilled holes on the stainless-steel casings were covered using Kapton tape to prevent exposure to the environment (as per the usual procedure used for such *operando* cells). The Na 'half' cells to be used for the *in-situ* synchrotron XRD studies were assembled a day prior to the experiments in order to carry them to the synchrotron facility at RRCAT, Indore, India.

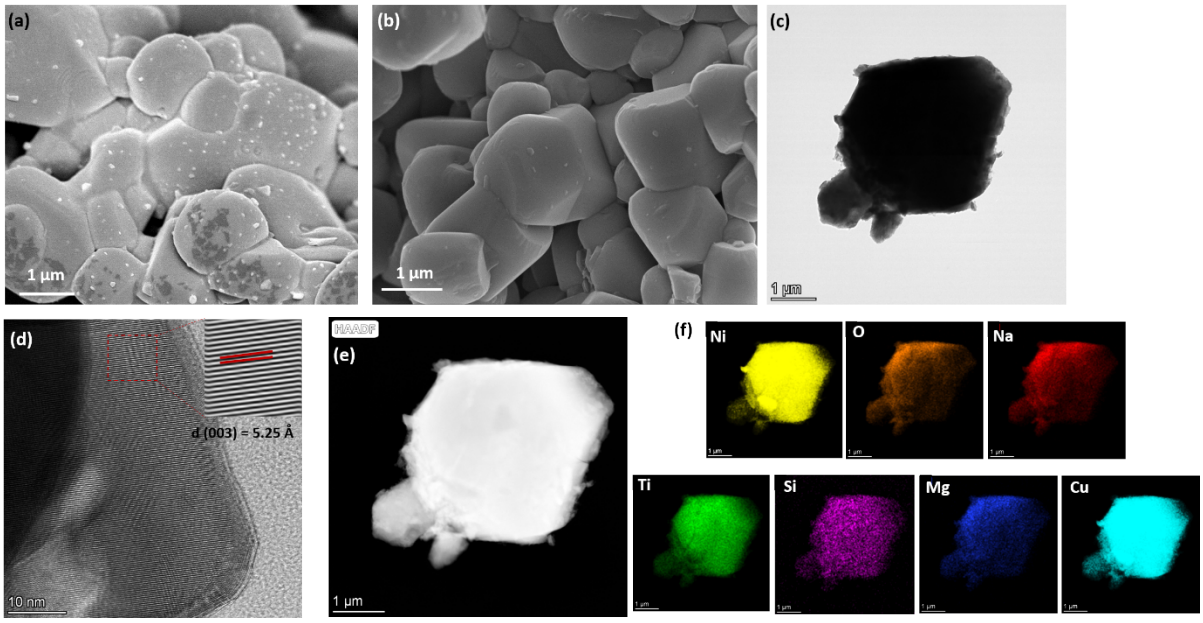

Fig. S1. Scanning electron micrograph (SEM) (a) Si-doped and (b) un-doped NaT_MO_2, (c) Bright field transmission electron micrograph, (d) High-resolution TEM image showing lattice fringes corresponding to the (003) planes and (e) HAADF-STEM image and (f) Elemental maps, as obtained with STEM-EDS, showing the distribution of all the elements in the as-synthesized $Na(Li_{0.05}Ni_{0.3}Ti_{0.45}Si_{0.05}Cu_{0.1}Mg_{0.05})O_2$ (*i.e.,* Si-doped NaT_MO_2).

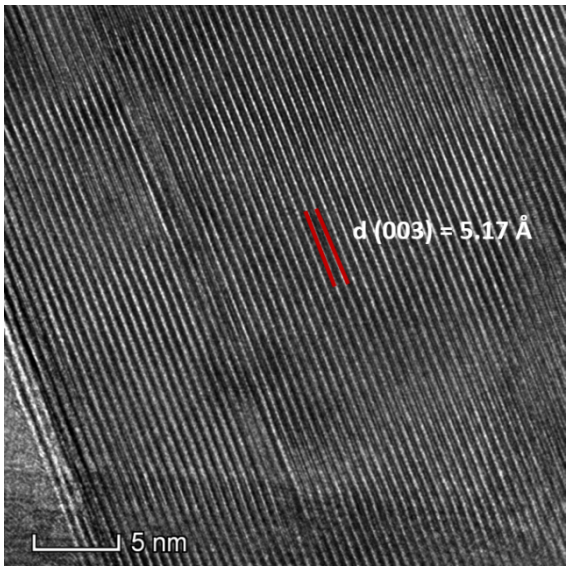

Fig. S2. High-resolution TEM image showing lattice fringes corresponding to the (003) planes of the as-synthesized $Na(Li_{0.05}Ni_{0.3}Ti_{0.5}Cu_{0.1}Mg_{0.05})O_2$ (*i.e.,* un-doped NaT_MO_2).

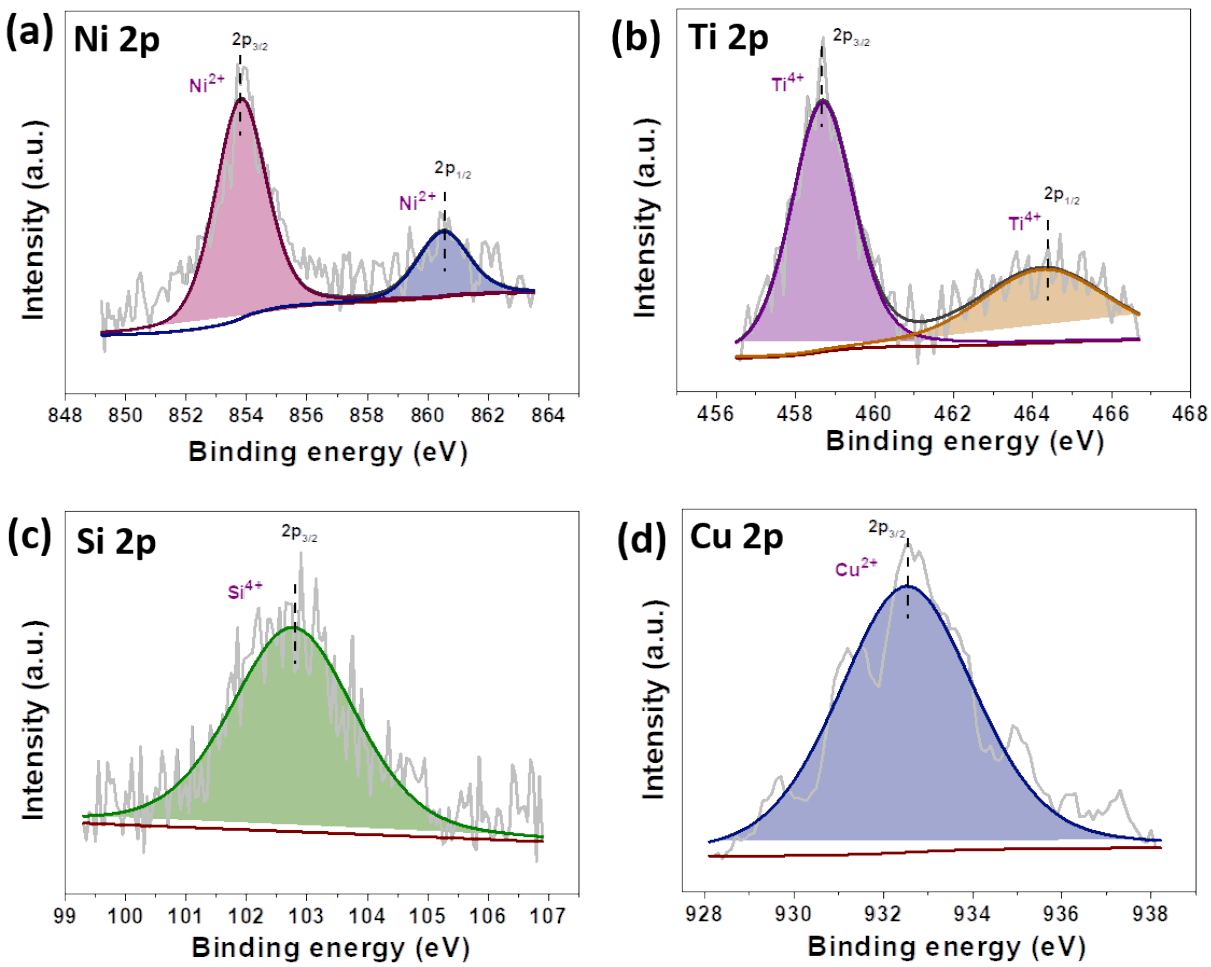

Fig. S3. (a) Ni 2p, (b) Ti 2p, (c) Si 2p and (d) Cu 2p XPS spectra obtained from the as-synthesized $Na(Li_{0.05}Ni_{0.3}Ti_{0.45}Si_{0.05}Cu_{0.1}Mg_{0.05})O_2$ (*i.e.,* Si-doped NaT_MO_2).

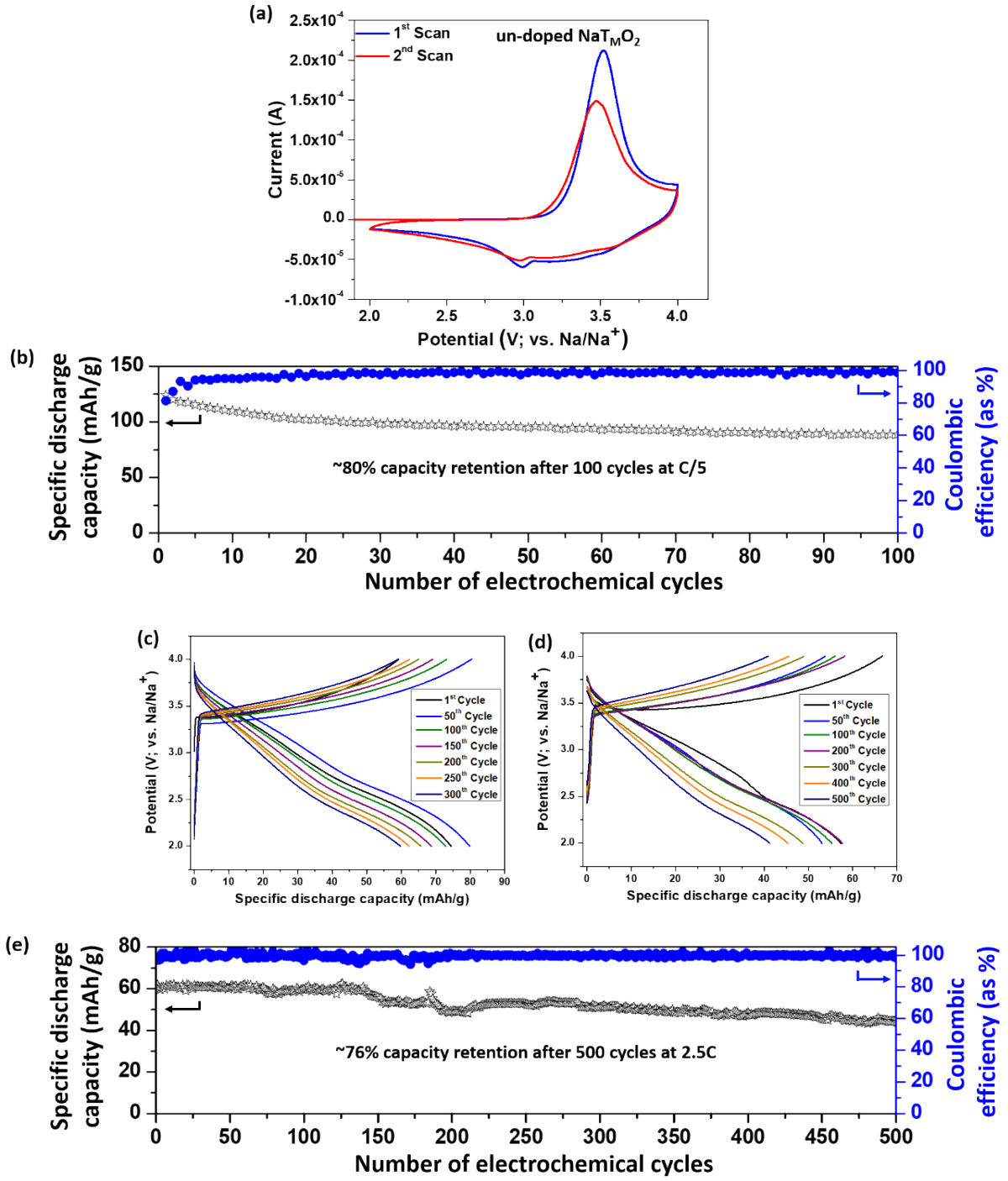

Fig. S4. (a) Cyclic voltammograms for the first two scans (@ 0.1 mV/s) of the as-synthesized $Na(Li_{0.05}Ni_{0.3}Ti_{0.5}Cu_{0.1}Mg_{0.05})O_2$ (*i.e.,* un-doped NaT_MO_2) based cathode in Na 'half' cell. (b) Cyclic stability, *i.e.,* reversible Na-storage capacity vs. cycle number (along with coulombic efficiency), obtained upon galvanostatic cycling at current densities equivalent to C/5 for 100 cycles; Potential profiles (*i.e.,* potential vs. specific capacity plots) for the selected galvanostatic charge/discharge cycles at current densities equivalent to (c) 1C, (d) 2.5C; (e) Cyclic stability, *i.e.,* reversible Na-storage capacity vs. cycle number (along with coulombic

efficiency), obtained upon galvanostatic cycling at a current density equivalent to 2.5C for 500 cycles (where 1C = 150 mA/g) of the as-synthesized $Na(Li_{0.05}Ni_{0.3}Ti_{0.45}\mathbf{Si}_{0.05}Cu_{0.1}Mg_{0.05})O_2$ based cathode (*i.e.,* Si-doped NaT_MO_2) in Na 'half' cell.

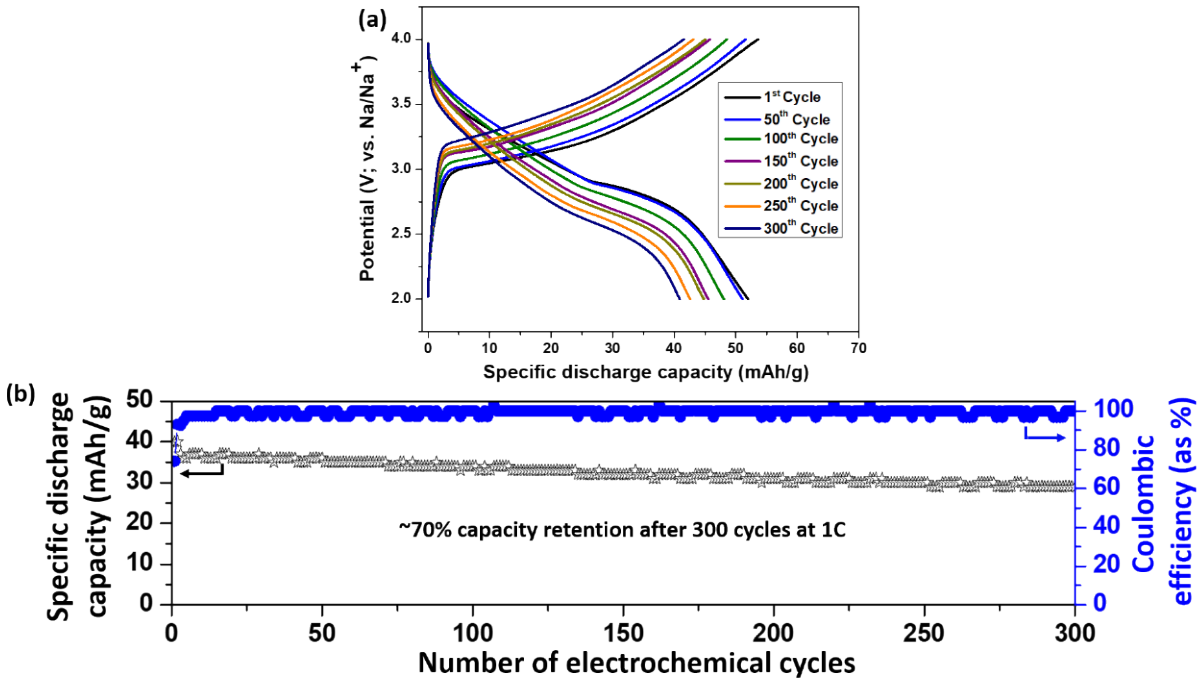

Fig. S5. (a) Potential profiles (*i.e.,* potential vs. specific capacity plots) for selected galvanostatic charge/discharge cycles and (b) Cyclic stability, *i.e.,* reversible Na-storage capacity vs. cycle number (along with coulombic efficiency), as obtained upon galvanostatic cycling @ 1C for 300 cycles of $Na(Li_{0.05}Ni_{0.3}Ti_{0.5}Cu_{0.1}Mg_{0.05})O_2$ (*i.e.,* un-doped NaT_MO_2) based cathode in Na 'half'.

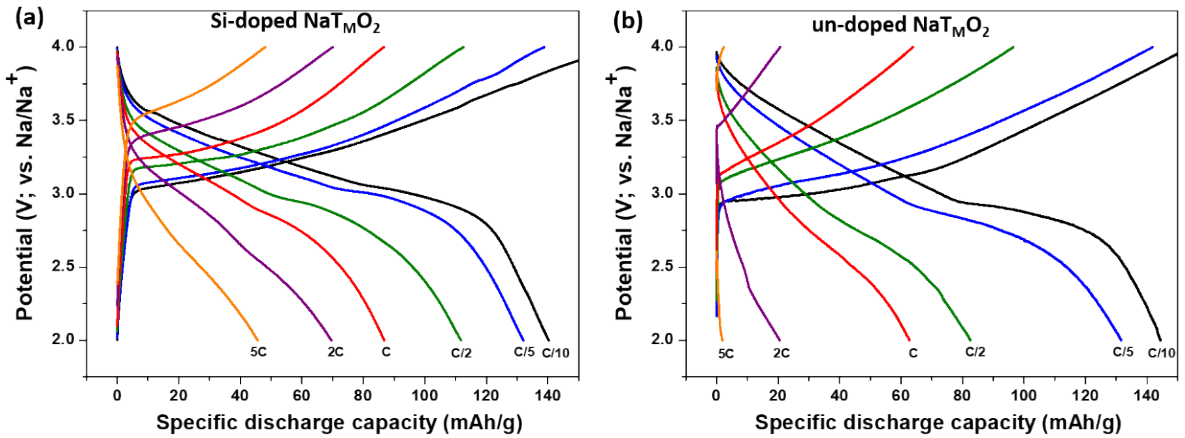

Fig. S6. Potential profiles (*i.e.,* potential vs. specific capacity plots) obtained at different current densities (as C-rates) for the (a) $Na(Li_{0.05}Ni_{0.3}Ti_{0.45}\mathbf{Si}_{0.05}Cu_{0.1}Mg_{0.05})O_2$ (*i.e.,* Si-doped NaT_MO_2) and (b) $Na(Li_{0.05}Ni_{0.3}Ti_{0.5}Cu_{0.1}Mg_{0.05})O_2$ (*i.e.,* un-doped NaT_MO_2) based cathodes in Na 'half' cells.

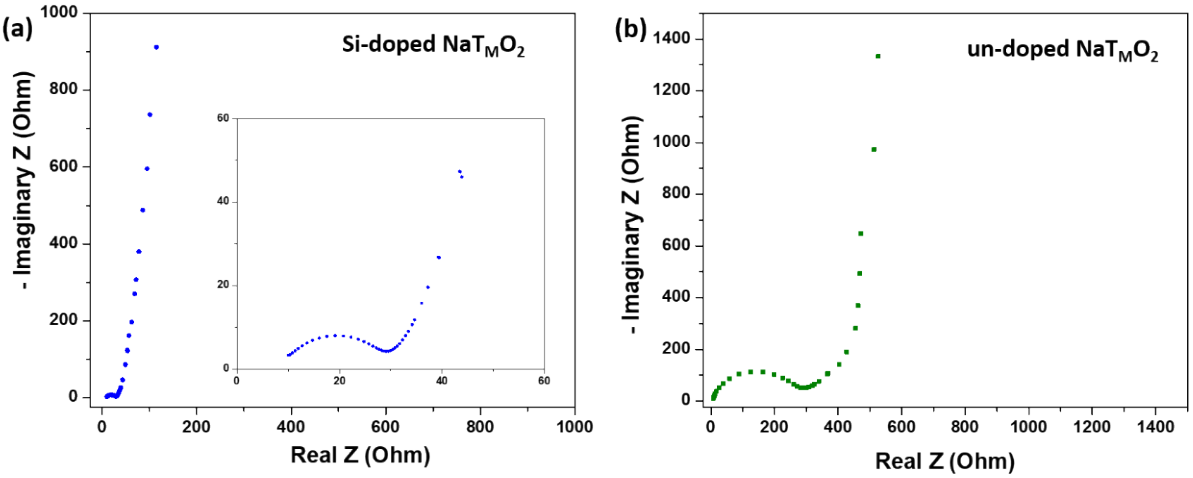

Fig. S7. Electrochemical impedance spectra (*i.e.,* Nyquist plots) obtained from the as-synthesized (a) Si-doped and (b) un-doped NaT_MO_2s, which have also been used for the estimation of Na-diffusivities.

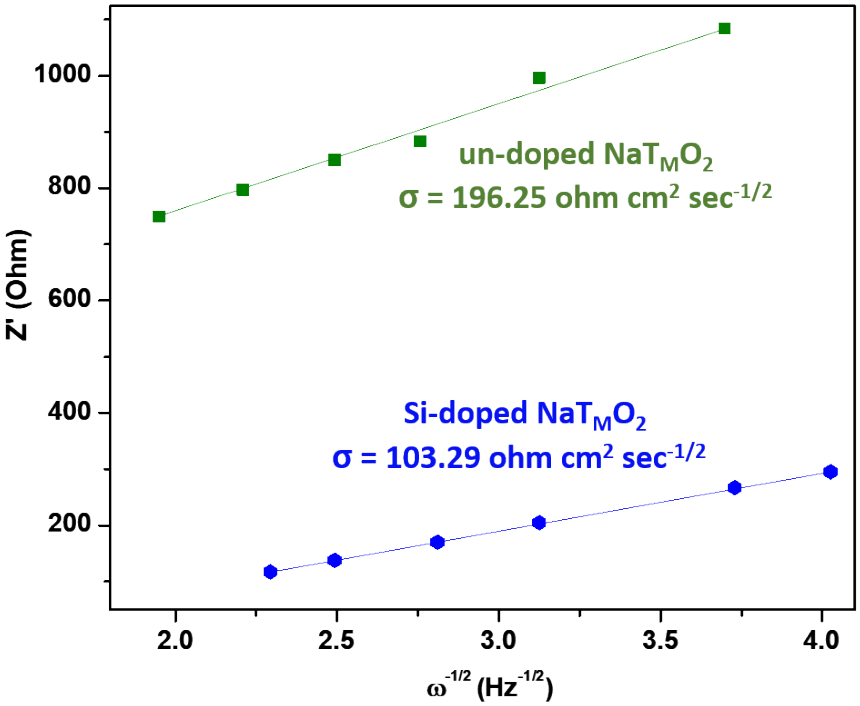

Fig. S8. Plot presenting the estimation of slope (σ) based on the data points obtained from the low frequency region of the corresponding EIS spectrum for the as-developed un-doped and Si-doped NaT_MO_2s.

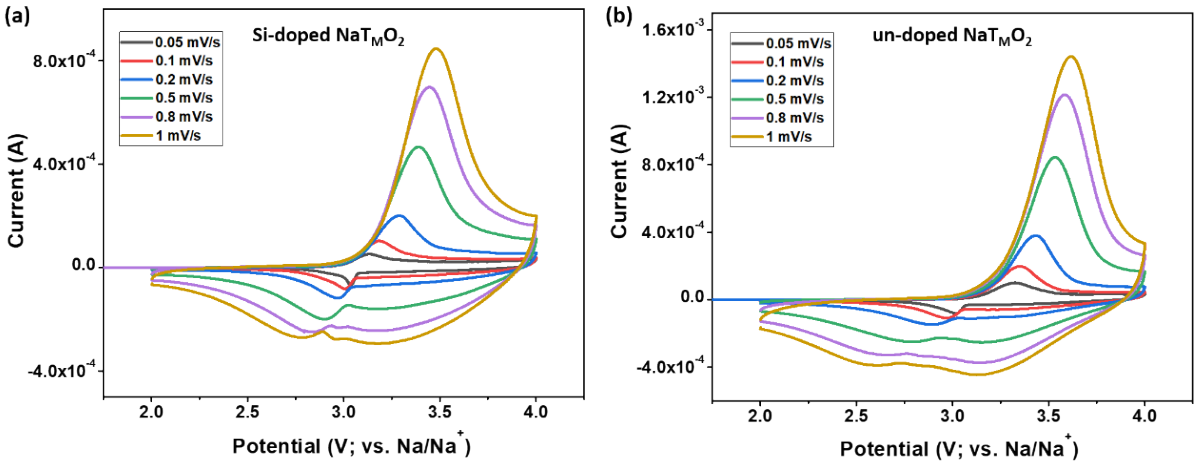

Fig. S9. Cyclic voltammograms obtained at different potential scan rates for the purpose of estimation of Na-diffusivity in the as-synthesized (a) Si-doped and (b) un-doped NaT_MO_2s.

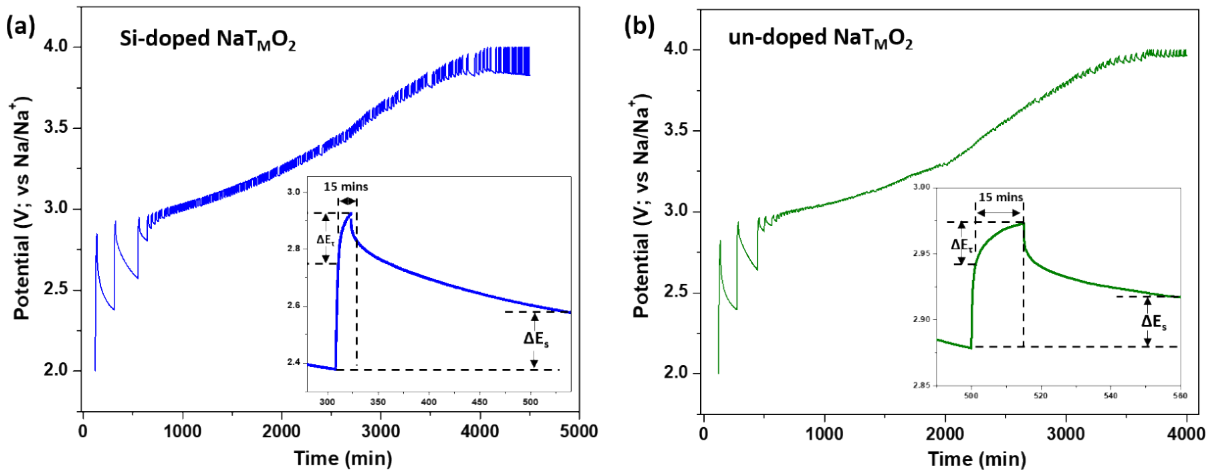

Fig. S10. Galvanostatic intermittent titration (GITT) profiles obtained during desodiation of the (a) Si-doped and (b) un-doped NaT_MO_2s while charging within a potential window of 2.0-4.0 V (vs. Na/Na^+), as has also been used for the estimation of Na-diffusivities.

Table S1. Chemical compositions (as per ICP-AES data) of the un-doped and Si-doped NaT_MO_2s.

O3-structured NaT_MO_2	**Na**	**Li**	**Ni**	**Si**	**Ti**	**Cu**	**Mg**
$Na(Li_{0.05}Ni_{0.3}Ti_{0.5}Cu_{0.1}Mg_{0.05})O_2$	0.97	0.048	0.3	-	0.46	0.095	0.043
$Na(Li_{0.05}Ni_{0.3}Ti_{0.45}\mathbf{Si}_{0.05}Cu_{0.1}Mg_{0.05})O_2$	0.94	0.043	0.3	0.046	0.42	0.098	0.049
error	0.028	0.003	0.005	0.0026	0.018	0.0027	0.0015

Table S2. Structural parameters obtained from Rietveld refinement of the XRD pattern corresponding to the un-doped NaT_MO_2 [*i.e.,* $Na(Li_{0.05}Ni_{0.3}Ti_{0.5}Cu_{0.1}Mg_{0.05})O_2$].

Element	**X**	**Y**	**Z**	**Chemical occupancy**	**Wykoff**
Na	0	0	0.5	1.03	3b
Cu	0	0	0	0.992	3a
Li	0	0	0	0.048	3a
Ni	0	0	0	0.29	3a
Mg	0	0	0	0.042	3a
Ti	0	0	0	0.483	3a
O	0	0	0.264	1	6c
a = b = 3.014 A		**c = 16.056 A**	**χ^2 = 4.54**		

Table S3. Structural parameters obtained from Rietveld refinement of the XRD pattern corresponding to the Si-doped NaT_MO_2 [*i.e.,* $Na(Li_{0.05}Ni_{0.3}Ti_{0.45}\mathbf{Si}_{0.05}Cu_{0.1}Mg_{0.05})O_2$].

Element	**X**	**Y**	**Z**	**Chemical occupancy**	**Wykoff**
Na	0	0	0.5	0.997	3b
Cu	0	0	0	0.092	3a
Li	0	0	0	0.044	3a
Ni	0	0	0	0.29	3a
Mg	0	0	0	0.045	3a
Si	0	0	0	0.047	3a
Ti	0	0	0	0.432	3a

O	0	0	0.267	1	6c
a = b = 3.0063 A	**c = 16.102 A**	**χ^2 = 2.03**			

Table S4. Comparison of the rate-capability of the as-developed Si-doped NaT_MO_2 with other O3-structured NaT_MO_2-based cathode materials reported to-date (including the un-doped NaT_MO_2 counterpart under consideration here) in terms of % drop in Na-storage capacity upon increase in C-rate from the lowest (~0.05C-0.2C) to the highest (~1C-5C) C-rate used and cycled under similar electrochemical conditions.

O3-structured NaT_MO_2	**Lowest C-rate used / specific capacity (in mAh/g)**	**Highest C-rate used / specific capacity (in mAh/g)**	**% drop in Na-storage capacity b/w the lowest and highest C-rates**	**Ref.**
$NaNi_{0.5}Mn_{0.5}O_2$	0.05C / 141	2C / 80	44	1
$NaLi_{0.05}(Ni_{0.25}Fe_{0.25}Mn_{0.5})_{0.95}O_2$	0.1C / 180.1	5C / 96.2	47	2
$Na(Ni_{0.25}Fe_{0.25}Mn_{0.5})O_2$	0.1C / 177.5	5C / 50	71.8	2
$Na(Ni_{0.4}Fe_{0.2}Mn_{0.2}Ti_{0.2})O2$	0.1C / 145	2C / 45	68.9	3
$Na(Ni_{0.33}Li_{0.11}Ti_{0.56})O_2$	0.2C / 91	2C / 48	48	4
$Na(Fe_{0.5}Ni_{0.5})O_2$	0.2C / 126	2C / 60	52	5
$Na(Cu_{0.2}Fe_{0.27}Mn_{0.53})O_2$	0.1C / 140	2C / 75	46	6
$Na_{0.8}(Li_{0.2}Fe_{0.2}Mn_{0.6})O_2$	0.1C / 170	3C / 70	58.8	7
$Na(Ni_{0.2}Fe_{0.35}Mn_{0.4}Zn_{0.05})O_2$	0.05C / 148	2C / 68	54	8
$Na(Mn_{0.5}Ni_{0.2}Fe_{0.3})O_2$	0.05C / 140	2C / 50	64	9
$Na(Mn_{0.48}Ni_{0.2}Fe_{0.3}Mg_{0.02})O_2$	0.05C / 160	2C / 70	56.3	9
$Na(Ni_{0.45}Mn_{0.3}Ti_{0.2}Zr_{0.05})O_2$	0.05C / 146	2C / 78	47	10
$Na(Li_{0.05}Ni_{0.3}Ti_{0.5}Cu_{0.1}Mg_{0.05})O_2$	0.2C / 141	1C / 45	68	**This work**
$Na(Li_{0.05}Ni_{0.3}Ti_{0.45}Si_{0.05}Cu_{0.1}Mg_{0.05})O_2$	0.2C / 128	2.5C / 73	**42.9**	

References

1 P. Wang, Y. You, Y. Yin and Y. Guo, *J. Mater. Chem. A*, 2016, **4**, 17660–17664.

2 S. -M. Oh, S. -T. Myung, J. -Y. Hwang, B. Scrosati, K. Amine and Y. -K. Sun, *Chem. Mater*, 2014, **05**, 6165–6171.

3 X. Sun, Y. Jin, C. Y. Zhang, J. W. Wen, Y. Shao, Y. Zang and C. H. Chen, *J. Mater. Chem. A*, 2014, **2**, 17268–17271.

4 S. Zhang, Y. Liu, N. Zhang, K. Zhao, J. Yang and S. He, *J. Power Sources*, 2016, **329**, 1–7.

5 D. Asakura, H. Niwa, H. Kiuchi, J. Miyawaki and Y. Harada, *Chem. Mater*, 2016, **28**, 1058–1065.

6 S. -M. Oh, P. Oh, S. -O. Kim and A. Manthiram, *J. Electrochem. Soc.*, 2017, **164**, A321–A326.

7 L. Yang, J. Miguel, Z. Shadike, S. Bak, F. Bonilla, P. K. Nayak, J. R. Buchheim, X. Yang, T. Rojo and P. Adelhelm, *Adv. Funct. Mater.*, 2020, **30**, 2003364.

8 Q. Mao, C. Zhang, W. Yang, J. Yang, L. Sun, Y. Hao and X. Liu, *J. Alloys Compd.*, 2019, **794**, 509–517.

9 C. Zhang, R. Gao, L. Zheng, Y. Hao and X. Liu, *ACS Appl. Energy Mater.*, 2018, **10**, 10819–10827.

10 M. Leng, J. Bi, W. Wang, Z. Xing, W. Yan, X. Gao, J. Wang and R. Liu, *J. Alloys Compd.*, 2020, **816**, 152581.

Section S2. Procedures adopted for the estimation of Na-diffusivities

Detailed description concerning estimation of Na-diffusivity from electrochemical impedance spectroscopy (EIS)

The straight-line parts in the low frequency regions of electrochemical impedance spectra (as in Fig. S4), as obtained for the Si-doped and un-doped NaT_MO_2s, have been considered for the estimation of the Na-diffusivities.

The plots for the Z_{real} vs. reciprocal square root of the frequency ($\omega^{-1/2}$) corresponding to the low frequency regions for both Si-doped and un-doped NaT_MO_2s (as shown in Fig. S5) yield straight lines with slopes (σ), as per the following equation;

$$Z_{real} = R_{sol} + R_{ct} + \sigma\omega^{-1/2} \ldots\ldots. (1)$$

The apparent Na-diffusivity (D_{Na+}) is estimated as per the following equation;

$$D_{Na+} = (R^2T^2) / (2A^2n^4F^4C^2\sigma^2) \ldots\ldots\ldots (2)$$

where, R is the universal gas constant, T is the temperature, A is surface area of the electrode, n is the number of electrons involved in charge transfer, F is the Faraday constant, C is the concentration of Na-ions in the electrolyte and σ is the slope obtained from eq. (1).

Detailed description concerning estimation of Na-diffusivity from Cyclic voltammetry

Cyclic voltammetry scans, with different potential scan rates ranging from 0.05 to 0.35 mV/s, were conducted with the Si-doped and un-doped NaT_MO_2 based electrodes. The cyclic voltammograms obtained with both the materials at the different scan rates are presented in Fig. S6, which shows an increase in peak current (I_P) with increase in scan rate (υ). The anodic current peaks were taken into consideration for estimating the Na-ion diffusivity (D_{Na^+}), as per the Randles–Sevcik equation, as below;

$$D_{Na^+} = (I_p) / (2.69x10^5 * n^{1.5} * A * C * \upsilon^{0.5}) \ldots\ldots\ldots (3)$$

where, I_p is the peak current, n is the number of electrons involved in redox reaction, A is the surface area of the electrode, C is the concentration of Na-ions and υ is the potential scan rate.

Detailed description concerning estimation of Na-diffusivity from galvanostatic intermittent cycling technique (GITT)

According to Fick's 2nd law of diffusion, the diffusion coefficient of an alkali metal ion in an electrode material can be estimated from the following equation;

$D_{Na+} = (4/\pi\tau) * [(m_B*V_M)/(M_B*A)]^2 * (\Delta E_s/\Delta E_t)^2$ ……. (4)

where, τ is the duration of the current pulse, m_B is mass of the active material, V_M is the molar volume of the material, M_B is the molar mass of the material and A is the surface area of the electrode, with ΔE_s and ΔE_t been estimated from the GITT profile, as indicated in Fig. S7.